Heliyon 10 (2024) e23199

Contents lists available at ScienceDirect

Heliyon

journal homepage: www.cell.com/heliyon

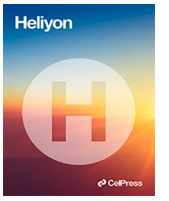

Synthesis of Sn doped and rice husk derived activated carbon surface coating NMC 811 through solution combustion method

Fiona Angellinnov [a], Achmad Subhan [b], Alan J. Drew [c], Anne Z. Syahrial [a,*]

[a] Department of Metallurgical and Materials Engineering, Faculty of Engineering, Universitas Indonesia, Depok, 16424, Indonesia
[b] Research Centre for Advanced Materials-National Research and Innovation Agency, South Tangerang, 15314, Indonesia
[c] School of Physics and Chemical Science, Queen Mary University of London, G O Jones Building, 327 Mile End Road, London, E1 4NS, UK

ARTICLE INFO

Keywords:
Activated carbon coating
Lithium-ion battery cathode
NMC 811
Rice husk
Sn doping

ABSTRACT

Nickel rich cathode material is widely used in lithium-ion batteries due to its high capacity, low cost, and environmentally friendly. However, high nickel content leads to capacity decay, poor rate capability, thermal and structural instability. To overcome these drawbacks, in this work, nickel rich NMC 811 was doped with tin to form $LiNi_{0.8}Mn_{0.1}Co_{0.1-x}Sn_xO_2$ with x = 0.01, 0.03, 0.05 via solution combustion method. Crystal structure, morphology, particle size, surface area and electrochemical performance were characterized and analyzed. The optimum Sn-doped NMC 811 was further surface modified with rice husk derived activated carbon. Electrochemical characterization showed that dual modification with 3% Sn-doping and rice husk derived activated carbon coating (NMC-Sn/C) provided the highest conductivity of 1.73×10^{-4} S/cm, which was higher than that of NMC without modification (1.88×10^{-5} S/cm). The capacity reached 84.60 mAh/g with retention of 75% after 50 cycles. These improvements originate from the stabilizing effect of Sn-doping and rice husk derived activated carbon coating that reduces the direct contact between NMC 811 and electrolyte. Hence, modifications with Sn-doping and rice husk derived activated carbon coating are promising to enhance the electrochemical performance of NMC 811.

1. Introduction

The extensive use of fossil fuel causes air pollution because of carbon dioxide emission, which leads to the climate change [1]. This emission affects not only the environment, but also human health [2]. The source of this fossil fuel is nonrenewable and can be depleted over the years. Due to these concerns, a renewable energy source is needed to fulfill the energy demand of clean energy.

For the use of clean energy, there is now a trend towards wider use of electric cars in which the use of batteries is inevitable. Moreover, for electricity sources that come from solar energy, the use of batteries cannot be avoided because there is no sunlight at night. Energy storage system is also necessary since sustainable energies such as solar, wind, and hydroelectric power are affected by fluctuating atmosphere [3]. Lithium-ion batteries (LIB) has been considered as the most promising energy storage [4] and has been widely used as a power source in electronic devices and electric vehicles. This battery has high energy and power density, long life, and environmentally friendly [5]. The cathode, one of its components, accommodates fewer Li^+ ions per unit weight than that of the anode, and thus defines the maximum capacity of LIB [6].

* Corresponding author.
E-mail address: anne.zulfia@ui.ac.id (A.Z. Syahrial).

https://doi.org/10.1016/j.heliyon.2023.e23199
Received 12 August 2023; Received in revised form 26 November 2023; Accepted 29 November 2023
Available online 3 December 2023

One of lithium-based cathode materials is nickel manganese cobalt (NMC). This NMC has been widely studied because of its high reversible capacity, low cost, environmental friendliness, and strong structural stability [7]. This material is not only used in electric vehicles, but also in medical devices, power tools, and portable electronic devices [8]. Based on its nickel, manganese, and cobalt ratio, NMC 811 ($LiNi_{0.8}Mn_{0.1}Co_{0.1}O_2$) exhibits higher capacity, less toxicity, and lower cost compared to the other NMC [9]. However, the high nickel content in NMC 811 leads to severe capacity degradation, poor rate capability, thermal and structural instability, and safety problems [10]. Similar ionic radii of Ni^{2+} and Li^+ (0.76 and 0.69 Å, respectively) causing Ni^{2+} to occupy Li^+ site during charge discharge, leading to capacity loss [11]. Besides that, when exposed to air, NMC 811 could take up H_2O and CO_2 [12] because excess lithium on the surface will react with these compounds resulting in LiOH and Li_2CO_3 [13]. These lithium compounds impurities hinder Li^+ diffusion and react with $LiPF_6$ electrolyte generating hydrogen fluoride (HF) gas that result in the dissolution of transition metal in NMC structure [8]. Fortunately, these problems could be tackled by using different raw materials and optimizing the synthesis method, doping with other metal elements, and coating on the surface [14].

Many investigators have used metallic elements to increase structural stability and electrochemical performance of NMC such as W [15], Al [16,17], Fe [16], and Sn [18,19]. Compared to other metals, tin (Sn) was known to give the highest rate-capability and longest life cycle (>20%) [16]. Tin doping contributes to better interface and structural stability of lithium-rich NMC resulting in excellent discharge capacity of 250.2 mAh/g [20]. Appropriate Sn doping into nickel rich NMC improves the cycling stability, showing capacity retention of 92.9% after 100 cycles [21]. Modification of NMC 811 with Sn as dopant and coating provided capacity retention of 96.6% and 93.7%, respectively, after 270 cycles [18]. Dual modification of Sn and Ag coating provided discharge capacity of 193.3 mAh/g with retention of 89.4% after 90 cycles, which is better than NMC 811 without modification (183.7 mAh/g, 87.9%) [22]. Besides metal, carbon could also be used as coating material for NMC. In addition to reducing direct contact between NMC and electrolyte, carbon could enhance the electron transfer [23]. Super P carbon black [24] and dopamine hydrochloride [25] were known to give higher rate capability and performance than that of NMC 811 without coating, because carbon coat protects NMC 811 from side reactions between the electrolyte/NMC 811. PVDF as carbon source has also been studied [26] and the results showed that 4 nm thick coating layer on the NMC 811 surface improved the rate capacity and cyclability. Other than these sources, carbon could also be obtained from renewable sources such as biomasses [27].

One of biomasses that is readily available in Indonesia is rice husk, since Indonesia is a paddy cultivating country. Rice husk is a byproduct of rice production, where 1000 kg of paddy rice produce 200 kg of rice husk [28]. This huge amount of rice husk waste could be used as a cheap and renewable source of carbon since rice husks contain around 37–54% carbon [29]. In this work, considering the drawbacks of NMC 811, we modified NMC 811 using Sn as a doping and rice husk derived activated carbon as a coating material. To the best of authors' knowledge, there has not been an article discussing this dual modification on NMC 811. We compared the amount of Sn doping into NMC 811 through solution combustion method. The characteristics of NMC 811 with and without Sn-doping were evaluated. Further, Sn-doped NMC 811 that provided the best performance was coated using rice husk derived activated carbon. The results are presented and discussed in detail.

2. Material and methods

2.1. Preparation of rice husk activated carbon

Preparation of activated carbon was based on the work of other [30] with some modifications and is explained as the following. Rice husk was collected from a paddy field and was cleaned using running water to remove any remaining dirt and was air-dried. Clean rice husks were carbonized at 400 °C for 3 h to form char. This sample was named inactivated carbon. The obtained char was soaked for 24 h in sodium hydroxide (NaOH 13%, Merck) and activated in a tubular furnace at 850 °C for 2 h. The sample was neutralized (pH

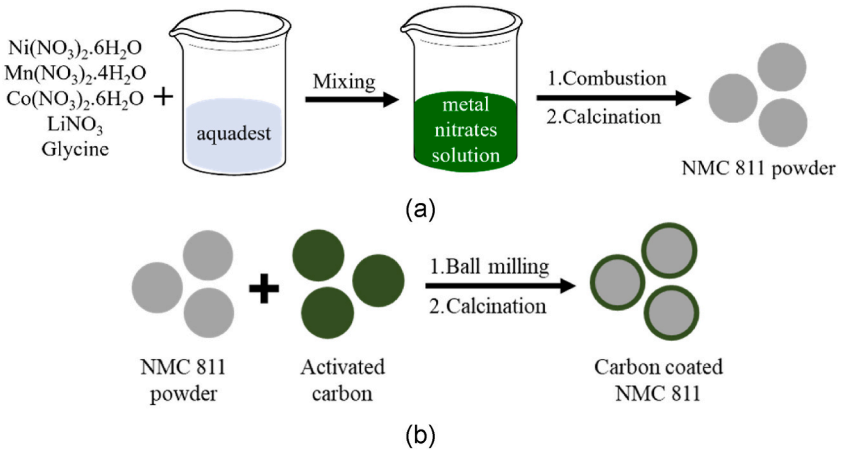

Fig. 1. (a) Schematic of the solution combustion synthesis of NMC 811, and (b) the preparation of rice husk activated carbon coated NMC 811.

6–7) and dried for 12 h at 105 °C. The obtained carbon was labeled as activated carbon. Infrared spectroscopy (FTIR, Perkin Elmer), and Brunauer Emmett Teller (BET, Quantachrome) were used to characterize the inactivated and activated carbon.

2.2. Preparation of active materials

Solution combustion method was used to synthesize NMC 811 using metal nitrate precursors and glycine as fuel [31] as illustrated in Fig. 1(a). A stoichiometric amount of $LiNO_3$, $Ni(NO_3)_2.6H_2O$, $Mn(NO_3)_2.4H_2O$, $Co(NO_3)_2.6H_2O$, and glycine (all were purchased from Sigma Aldrich) were dissolved in distilled water and heated at 185 °C until a self-combustion occurred. The obtained powder was sintered for 4 h at 800 °C with heating rate of 4 °C/min to obtain the final product, labeled as NMC.

The synthesis of Sn-doped NMC 811 follows the same procedure. Three variations of Sn powders (Sigma Aldrich) 1, 3, and 5 wt% were prepared and each was added to the green aqueous solution of metal nitrates-glycine before heating. The combustion and sintering took place at the same temperature of 185 °C and 800 °C, respectively. The obtained powders were labeled as NMC-1, NMC-3, and NMC-5 for 1, 3, and 5 wt%, respectively.

Further, the activated carbon (5 wt%) was milled with NMC (illustrated in Fig. 1(b)), with ratio of zircon balls: materials 4:1 (w/w) at 300 rpm for 1 h. The powder was then calcined for 3 h at 300 °C, and labeled as NMC/C. The Sn-doped NMC having the best electrochemical performance was selected to be coated with 5 wt% rice husk derived activated carbon and labeled as NMC-Sn/C.

For characterization, BET, X-ray diffraction (XRD, PANalytical X'Pert PRO, K-α Cu of 1.54 A) in the 2θ range of 10°–90°, field emission scanning electron microscope equipped with energy dispersive X-ray spectroscopy (FESEM/EDS, FEI Inspect F-50), transmission electron microscope (TEM, FEI Tecnai G2 20 S-Twin), and particle size analyzer (PSA, Zetasizer Pro-Blue) were used.

2.3. Battery fabrication and electrochemical characterization

The active materials (NMC, NMC-1, NMC-3, NMC-5, NMC/C, and NMC-Sn/C) were mixed with polyvinylidene fluoride (PVDF, Gelon) and super P (Gelon), with a weight ratio of 8:1:1, respectively, and dissolved in N-methyl-2-pyrrolidone (NMP, Gelon). The resulting black slurry was then coated onto aluminum foil, dried at 70 °C for 2 h, and punched into circular area of 1.65 cm. Solution of 1 M lithium hexafluorophosphate dissolved in ethylene carbonate/dimethyl carbonate ($LiPF_6$ in EC/DMC), Celgard 2500, and metallic lithium were used as electrolyte, separator, and anode, respectively. The battery assembly in the forms of CR 2032-coin cell was conducted in a glove box filled with argon gas. Electrochemical impedance spectroscopy (EIS, Metrohm Autolab PGSTAT 302 N) was further carried out at an applied voltage of 100 mV in the frequency range of 0.1–50 kHz. Cyclic voltammetry (CV) test was conducted at a scan rate of 100 μV/s in the voltage range of 2.5–4.4 V (Wonatech, CCJ8F2-8 PS). Finally, charge discharge test was conducted for NMC-Sn/C at 1C for 50 cycles (Wonatech, CCJ8F2-8 PS).

3. Results and discussion

3.1. Rice husk derived activated carbon analysis

The FTIR spectra of inactivated and activated carbon shown in Fig. 2(a) indicate that the activation process using NaOH results in significant differences. The inactivated carbon shows several absorbances. The broad band between 3100 and 3600 cm^{-1} corresponds to the absorbance of –OH from water [30]. Stretching vibration of C=O from carboxylic group and C=C from the aromatic ring are at 1695 cm^{-1} and 1573 cm^{-1}, respectively [32]. Absorbance of the symmetric and asymmetric stretching of Si-O are found at 1076 cm^{-1} and 800 cm^{-1}, respectively [33] whereas bending vibration of Si-O-Si is detected at 448 cm^{-1} [34]. Meanwhile, the activated carbon shows no absorbance. This could be due to the decomposition of volatile compounds in carbon, leaving only carbon [30]. A similar result was observed in the work of Shrestha et al. [32] in which they activated NaOH-impregnated rice husk at 900 °C, and the resulting

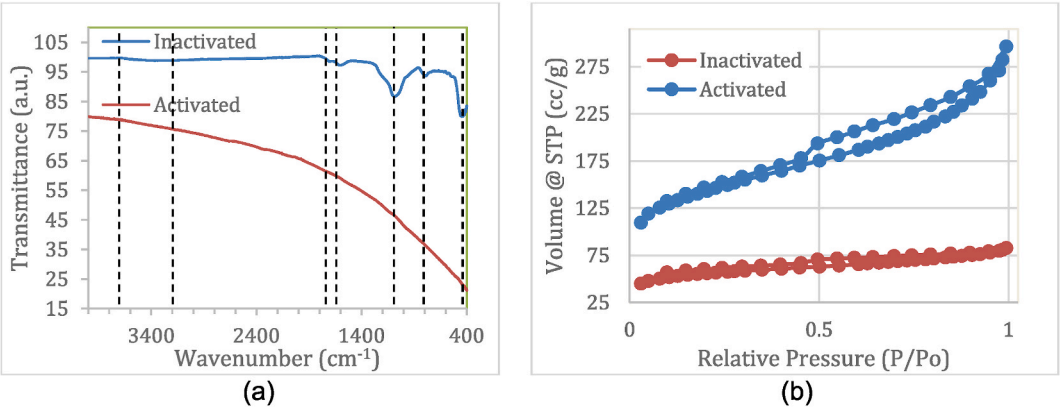

Fig. 2. (a) FTIR spectra and (b) adsorption isotherm of inactivated and activated carbons.

infrared spectrum shows almost no absorption. The disappearance of most functional groups is due to the high activation temperature. Based on this result, it confirms that the use of NaOH as activation agent removes silica and other functional groups leaving only carbon.

The decomposition of volatile matters opens the pore of carbon, and hence, the characterization was performed using N_2 adsorption-desorption using BET. The obtained curve is shown in Fig. 2(b). Before activation, the N_2 adsorption is low, and the curve can be classified as Type-I. After activation, the adsorption of N_2 is higher and the curve displays a mixture of Type-I and Type-IV adsorption isotherm and a hysteresis loop can be observed. Similar results were also observed in another work, where rice husk derived carbon was activated using NaOH at four different temperatures (650, 700, 750, and 800 °C) [35] and that increasing the activation temperature resulted in a wider hysteresis loop. Table 1 lists the surface area and average pore size of inactivated and activated carbons. The surface area and average pore size of activated carbon are 469.4 m^2/g and 2.0 nm, respectively, which are larger than that of inactivated carbon (117.0 m^2/g and 1.4 nm, respectively). The results in this study is similar to the result obtained in Ref. [30] with surface area of 429.8 m^2/g and average pore size of 2.7 nm. These significant increase in the surface area and the average pore size are due to the release of volatile components during the activation process [36], which confirms the infrared results.

3.2. Active materials analysis

Metal nitrates were used as precursors in the solution combustion method. Compared to other metal salts such as sulfates and carbonates, metal nitrates have lower decomposition temperature, good solubility in water, and efficient oxidizing power of NO_3^- groups, therefore they are more preferable in this method [37]. The mixture of metal nitrates, glycine, and water as solvent was heated until the combustion took place. During the combustion, glycine was oxidized into gases and the metal cations reduced into metal oxides [38]. Reactions between the metal nitrates and glycine are as follows [39].

$$LiNO_3 + 0.8Ni(NO_3)_2.6H_2O + 0.1Mn(NO_3)_2.4H_2O + 0.1Co(NO_3)_2.6H_2O + 2C_2H_5NO_2 + O_2 \rightarrow LiNi_{0.8}Mn_{0.1}Co_{0.1}O_2 + 4CO_2 + 2.5N_2 + 10.8H_2O \quad (1)$$

$$LiNO_3 + 0.8Ni(NO_3)_2.6H_2O + 0.1Mn(NO_3)_2.4H_2O + 0.09Co(NO_3)_2.6H_2O + 2C_2H_5NO_2 + 1.03O_2 + 0.01Sn \rightarrow LiNi_{0.8}Mn_{0.1}Co_{0.09}Sn_{0.01}O_2 + 4CO_2 + 2.49N_2 + 10.74H_2O \quad (2)$$

$$LiNO_3 + 0.8Ni(NO_3)_2.6H_2O + 0.1Mn(NO_3)_2.4H_2O + 0.07Co(NO_3)_2.6H_2O + 2C_2H_5NO_2 + 1.09O_2 + 0.03Sn \rightarrow LiNi_{0.8}Mn_{0.1}Co_{0.07}Sn_{0.03}O_2 + 4CO_2 + 2.47N_2 + 10.62H_2O \quad (3)$$

$$LiNO_3 + 0.8Ni(NO_3)_2.6H_2O + 0.1Mn(NO_3)_2.4H_2O + 0.05Co(NO_3)_2.6H_2O + 2C_2H_5NO_2 + 1.15O_2 + 0.05Sn \rightarrow LiNi_{0.8}Mn_{0.1}Co_{0.05}Sn_{0.05}O_2 + 4CO_2 + 2.45N_2 + 10.50H_2O \quad (4)$$

The obtained powder was characterized using XRD and the results are shown in Fig. 3(a). The diffractograms match with reference pattern of NMC 811 (ICDD 96-152-0790), with hexagonal crystal structure and space group of R-3m. It can be seen from the diffractograms that NMC, NMC-1, NMC-3, NMC-5 are all crystalline and possess sharp NMC 811 peaks at 2θ of 18, 36, 38, 44, 48, 58, 64, and 67° that corresponds to the plane (003), (101), (006), (104), (10 $\bar{5}$), (009), (10 $\bar{8}$), and (113), respectively. However, compared to commercial NMC, there are intensities differences at 2θ 18, 36, 38, 44°. Analysis showed that LNO ($LiNiO_2$, ICDD 96-152-5554), which has the same hexagonal crystal system, R-3m space group, and crystal plane as NMC, was also detected and results in difference peaks intensities. Further, intensities of the two highest peak (003) and (104) could be analyzed to determine the cation mixing between Li^+ and Ni^{2+}, where the ratio value higher than 1.2 resulting in better electrochemical performance [24,40,41]. In this work, as can be seen in Table 2, all samples including commercial NMC have ratio lower than 1.2. However, modification with rice husk derived activated carbon and Sn increased the ratio of NMC-3, NMC-5, and dual modification NMC-Sn/C, meaning that these modifications result in lower cation mixing compared to the sample without modification (pristine NMC). The dual modification sample (NMC-Sn/C) provided the highest ratio of 0.88. From the diffractograms in Fig. 3, it can also be seen that the use of Sn as dopant can substitute Co and did not change the crystal structure of NMC 811. However, in Fig. 3(b) for NMC-5 diffractogram, it can be observed a peak tailing at 2θ 44.8°. This has been confirmed to be Li_2SnO_3 phase (ICDD 96-100-8200), an impurity which was also observed in another work, where excess Sn as dopant in NMC 811 caused the formation of Li_2SnO_3 [22]. Therefore, in this work, among all the Sn amount used as dopant, 3% Sn doping is the optimum amount. In other words, the amount of Sn = 0.05 cannot be used as dopant for NMC 811. Mixing of NMC sample with activated carbon (5 wt%) resulted in a similar diffractogram pattern of NMC without activated carbon. In Fig. 3, it can be observed that NMC/C has peaks at the same 2θ as NMC sample. Also, there is no new peak found. It can be concluded that the addition of activated carbon to NMC 811 did not affect the crystal structure.

Fig. 4 shows the morphologies of NMC 811 synthesized via solution combustion and NMC 811 commercial. Compared to the commercial NMC (Fig. 4(c-d)) that has uniform spherical shaped particles, the NMC sample in Fig. 4(a and b) has some particles that

Table 1
Surface area and average pore size of inactivated and activated carbons.

Sample	Surface area (m^2/g)	Average pore radius (nm)
Inactivated	117.0	1.4
Activated	469.4	2.0

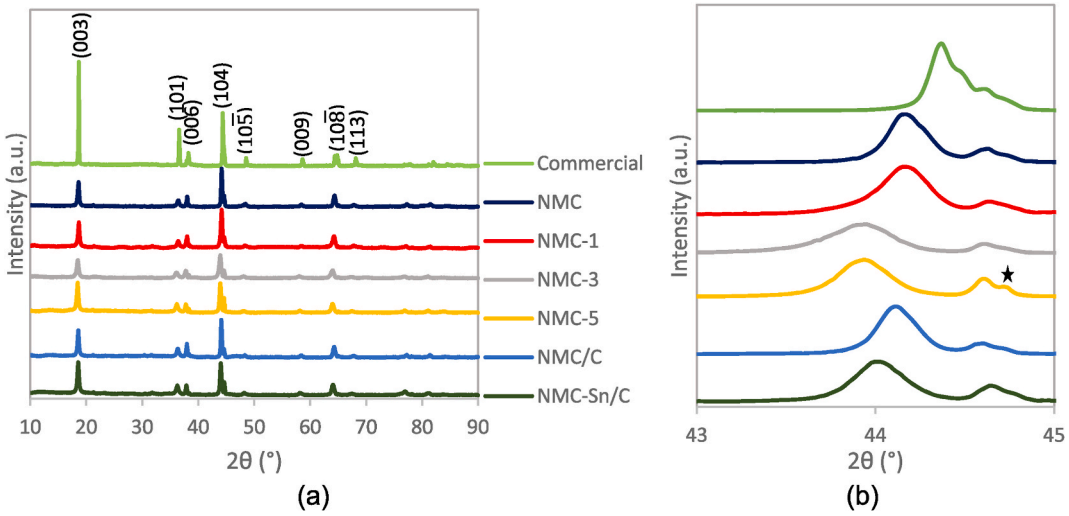

Fig. 3. (a) Diffractograms of NMC active materials and (b) enlarged at 2θ 43–45°.

Table 2
Ratio of I_{003}/I_{104} commercial NMC and synthesized NMC samples.

	Commercial	NMC	NMC-1	NMactC-3	NMC-5	NMC/C	NMC-Sn/C
I_{003}/I_{104}	1.15	0.59	0.57	0.76	0.62	0.50	0.88

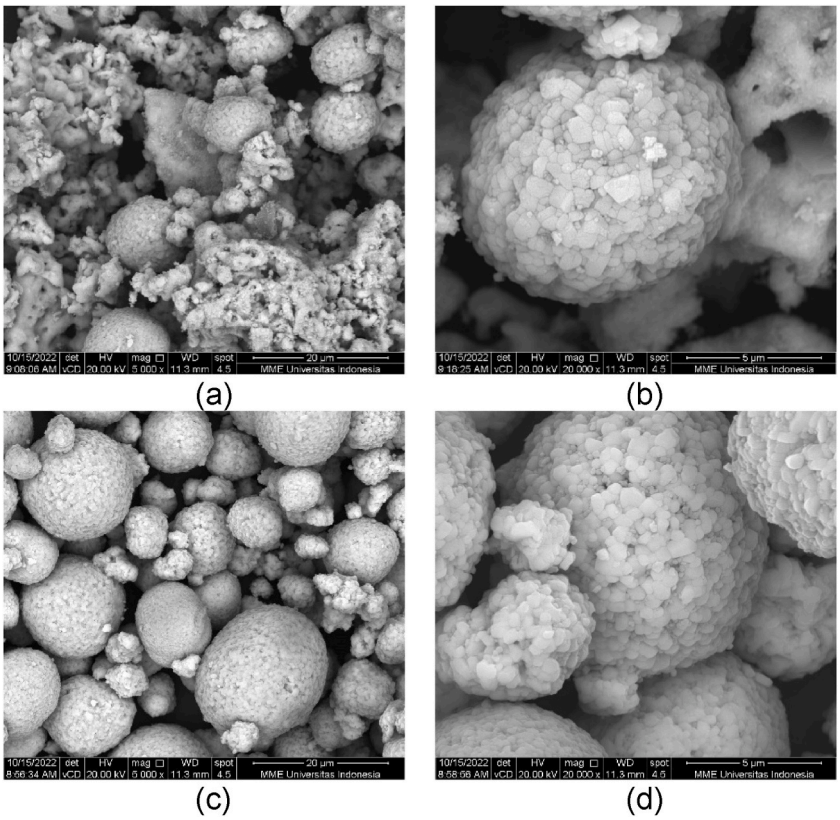

Fig. 4. Morphology of synthesized NMC 811 (a, b) and commercial NMC 811 (c, d).

formed a sphere shape while the others agglomerated into irregular shape. Some works from others also showed that this agglomeration is typical in NMC synthesized through solution combustion method using metal nitrate-glycine [31,42]. Pores can also be observed from the images. These pores increase the surface area, and thus increase the contact area between the electrolyte and NMC. It has also been found that pore increases the area for lithium ion insertion [43]. Further, NMC sample was characterized using BET and PSA. The results are given in Table 3. The obtained surface area is 11.89 m^2/g with an average particle size of 370.3 nm.

NMC sample was also characterized using EDS. Table 4 shows elemental composition of the active materials. The wt.% of nickel, manganese, cobalt, and oxygen detected are in accordance with the stoichiometric amount used. The mapping images of each element given in the supplement (Fig. S1(a–e)) show that the distribution is homogenous.

Fig. 5(a–f) shows the electron images of Sn-doped NMC. The morphologies are similar to that of NMC sample. The NMC particles aggregate with each other, resulting in an irregular shape, although the spherical shape can also be observed. The average particle size of NMC-1, NMC-3, and NMC-5 are 420.1, 491.4, and 533.2 nm, respectively, whereas the surface area is 37.07, 11.54, and 46.81 m^2/g, respectively. These results reveal that doping of Sn into NMC resulted in agglomeration and hence larger particle size and agree with the SEM images. It can be concluded that substitution of Co with Sn causes NMC to agglomerate thus larger particle size, and higher surface area because of the pores. Fig. 5(f) shows some smaller particles on the surface of NMC. These are Li_2SnO_3, which is also observed in another work [22]. These impurities contribute to the total surface area, which causes NMC-5 to have a larger surface area compared to NMC-1 and NMC-3 (Table 3). This is in accordance with the XRD result of NMC-5, where a new peak around 2θ 44.8° that belongs to Li_2SnO_3 phase can be observed.

Figs. S2(a–f), S3(a–f), and S4(a–f) show the elemental mapping of NMC-1, NMC-3, and NMC-5, respectively. For all samples, the distribution of nickel, manganese, cobalt, oxygen, and tin is homogenous. The composition of Sn detected from EDS shown in Table 4 is 1.46, 3.90, and 6.45 for NMC-1, NMC-3, and NMC-5, respectively, whereas the composition of Co is 7.97, 5.60, 4.44 wt%, respectively. These results agree with the stoichiometric amount used in the reaction.

The morphologies of NMC/C and NMC-Sn/C are shown in Fig. 6(a–d). Compared to NMC and Sn-doped NMC samples without activated carbon, these samples are less agglomerated. In Fig. 6(b) and (d), there are smaller particles on the surface of the larger particle. These smaller particles are the activated carbon that was added through solid state reaction method. To confirm that this is indeed the carbon layer on the NMC surface, TEM characterization was performed on NMC and NMC/C samples, and the results are given in Fig. 7(a) and (b). The NMC sample in Fig. 7(a) consists of dense particles, while amorphous coating layer is observed in NMC/C (Fig. 7(b)). The thickness of the carbon layer is estimated to be 0.55 nm. Analysis using BET and PSA of these samples is shown in Table 3. NMC/C surface area and average size are 30.48 m^2/g and 401.5 nm, respectively, while NMC-Sn/C are 22.36 m^2/g and 456.2 nm, respectively. The addition of activated carbon increased the overall surface area of NMC. This is due to the pore of the activated carbon.

EDS analyses were carried out for the activated carbon coated NMC and NMC-Sn, and the results are shown in Figs. S5(a–f) and S6 (a–g). The distribution of carbon in NMC/C and NMC-Sn is homogenous, as shown in Fig. S5(f) and Fig. S6(g). The other elemental compositions are also homogenously distributed. In Table 4, the composition of carbon is 6.10 wt% for NMC/C and 6.40 wt% for NMC-Sn/C, respectively. Meanwhile, the other elements are detected similar to that of NMC elemental composition. In another word, the addition of rice husk derived activated carbon to NMC and NMC-Sn did not affect the other elements. These results agree with the XRD results.

3.3. Electrochemical performance

Electrochemical impedance spectroscopy was used to investigate the influence of Sn-doping and rice husk derived activated carbon coating on the conductivity and diffusion coefficient of lithium-ion in NMC 811. Fig. 8 shows the Nyquist plots of all active materials. Each plot consists of a semicircle at high frequency and an inclined line at lower frequency. From the plots we can get R_{ct} values of all the active materials samples. This value was then calculated to get the conductivity using Equation (5), where σ is conductivity (S/cm), l is thickness of the sample (cm), R_{ct} is charge transfer resistance (Ω), and A is the active area (cm^2). Other than R_{ct}, we can also get R_s (solution resistance, Ω) value. The value of R_{ct}, R_s, real impedance (Z') and frequency (ω), can be calculated using Equation (6) to get the Warburg coefficient (σ_W) at low frequency by using Fig. 8(b). This coefficient further used to calculate the diffusion coefficient using Equation (7), where R is the gas constant (8.314 J/mol.K), T is the absolute temperature (298 K), A is the surface area of the electrode (2.1372 cm^2), F is the Faraday constant (96,500 C/mol), C is the concentration lithium-ion (4.37×10^{-3} mol/cm^3), and σ_w is the Warburg constant ($\Omega.cm^2/s^{1/2}$). The circuit shown in Fig. 8(a) was used to simulate and analyze the impedance spectra and the results are shown in Table 5.

Table 3
Surface area and average size of active materials analyzed using PSA.

Sample	Surface area (m^2/g)	Particle size (nm)
NMC	11.89	370.3
NMC-1	37.07	420.1
NMC-3	11.54	491.4
NMC-5	46.81	533.2
NMC/C	30.48	401.5
NMC-Sn/C	22.36	456.2

Table 4
Elemental composition of active materials.

Sample	Elemental composition (wt.%)					
	Ni	Mn	Co	O	Sn	C
NMC	60.00	7.44	8.55	23.95	–	–
NMC-1	66.80	8.19	7.97	15.58	1.46	–
NMC-3	59.52	7.44	5.60	23.54	3.90	–
NMC-5	59.66	7.53	4.44	21.92	6.45	–
NMC/C	52.16	6.72	7.36	27.65	–	6.10
NMC-Sn/C	58.83	7.24	5.47	18.56	3.50	6.40

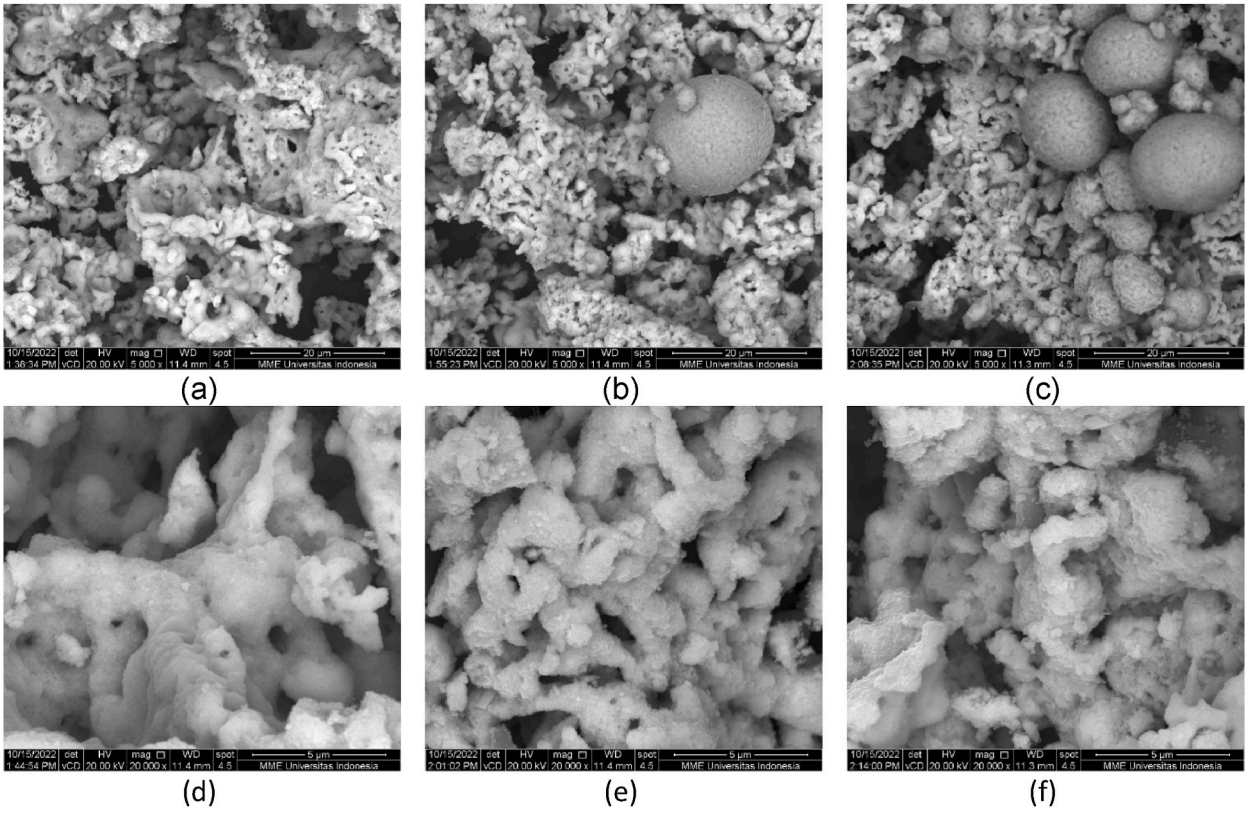

Fig. 5. SEM images of (a,d) NMC-1 (b,e) NMC-3 (c,f) NMC-5 scale bar 20 and 5 μm.

$$\sigma = l / R_{ct} A \tag{5}$$

$$Z' = R_s + R_{ct} + \sigma_w \, \omega^{-1/2} \tag{6}$$

$$D = 0.5\left(C\sigma_w \, AF^2\right)^2 \tag{7}$$

It can be seen from Table 5 that for the variation of Sn, NMC-3 showed the lowest R_{ct} value (285.97 Ω) and the highest conductivity (2.45×10^{-5} S/cm), higher than that of NMC-1 (419.19 Ω and 1.67×10^{-5} S/cm) and NMC-5 (506.97 Ω and 1.38×10^{-5} S/cm). This demonstrates the improved electron conductivity due to Sn doping that help stabilize bulk structure of NMC [44]. However, the diffusion coefficient of NMC-3 is lower than that of NMC-1 and NMC-5 (7.38×10^{-15}, 8.00×10^{-15}, and 2.09×10^{-14}). This could be due to the presence of Li_2SnO_3 impurities in NMC-5, which is also detected in XRD analysis. Sun et al. observed that this compound enhance lithium diffusion [22]. These results are lower compared to the work of Li et al. [18]. They obtained lithium diffusion coefficient of 3.49×10^{-13} for 2% Sn-modified NMC 811. This can be attributed to the cation mixing that is still present in the sample. However, our results still show that modification with Sn enhances the lithium diffusion and conductivity, compared to the one without Sn modification. For the C-coated NMC sample, NMC/C provided conductivity and diffusion coefficient of 1.46×10^{-4} S/cm and 4.16×10^{-13} cm^2/s, respectively. The increase in diffusion related to the pore that was observed in SEM images and confirmed by BET. Based on these results, NMC-3 was milled with 5 wt% activated carbon to obtain NMC-Sn/C and was analyzed using EIS. The

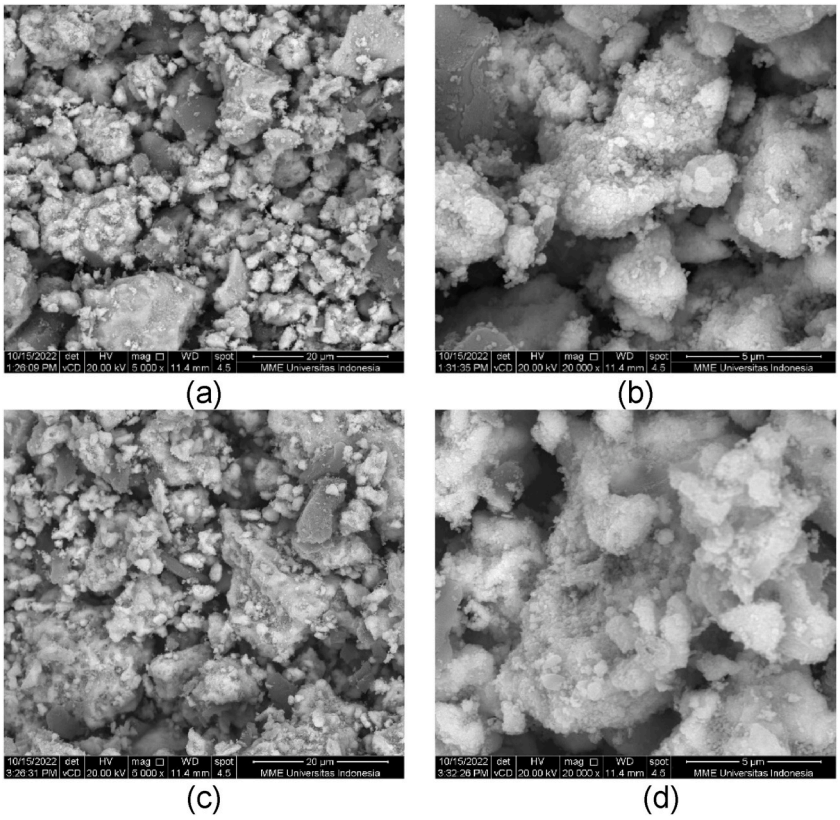

Fig. 6. SEM images of (a,b) NMC/C and (c,d) NMC-Sn/C scale bar 20 μm and 5 μm.

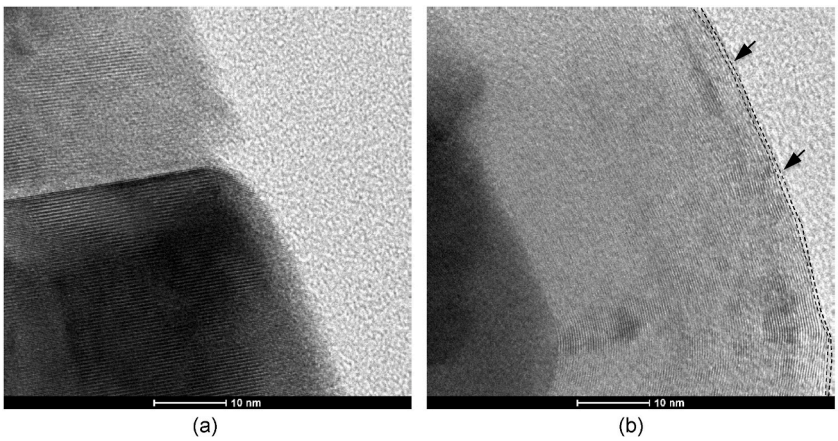

Fig. 7. High resolution TEM image of (a) pristine NMC and (b) activated carbon coated NMC, indicated by the arrows.

conductivity and diffusion coefficient of this dual modification sample (1.73×10^{-4} S/cm and 2.49×10^{-13} cm^2/s) are higher than single modification, both NMC-3 and NMC/C.

Cyclic voltammetry tests were conducted in the potential range of 2.5–4.4 V at scanning rate of 0.1 mV/s. The results are presented in Fig. 9 and Table 6. Peaks at around 4 V during the charging process for all samples corresponds to the oxidation of transition metals (Ni^{2+} to Ni^{4+} and Co^{3+} to Co^{4+}), and the reduction peaks observed below 3.5 V assigned to the reduction of Mn^{3+} to Mn^{4+} [39]. All Sn-doped NMC shows lower ΔE values than the one without doping. The lowest one is NMC-3 (720 mV). Similar with Sn-doped NMC, the carbon coated NMC sample shows lower ΔE than NMC without carbon, with potential difference value of 760 mV. Meanwhile, of all the samples, the NMC-Sn/C provided the lowest potential difference value (640 mV), and hence the lowest degree of polarization. These results agree with the EIS results.

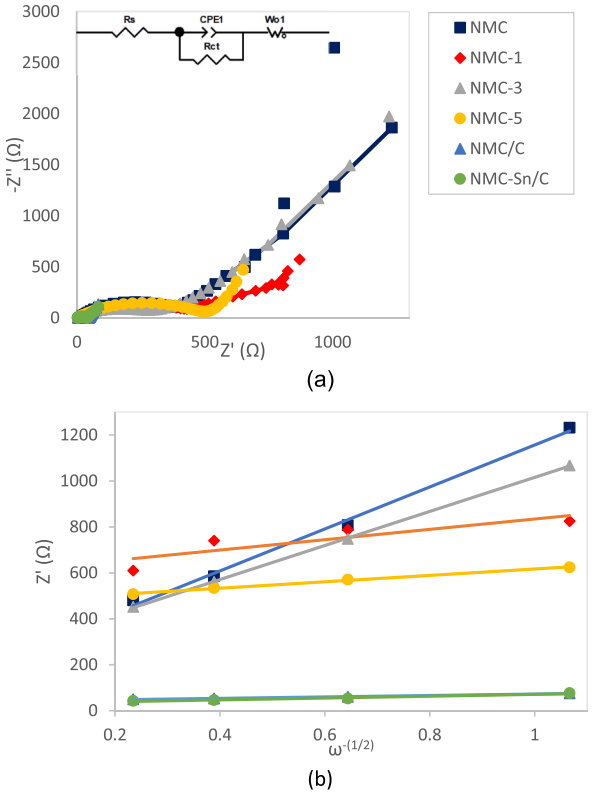

Fig. 8. (a) Nyquist plots of active materials, (b) graph of Z′ vs. $\omega^{-1/2}$ at the low-frequency region.

Table 5
Impedance parameters of active materials.

Sample	R_s (Ω)	R_{ct} (Ω)	σ (S/cm)	D (cm^2/s)
NMC	23.94	373.24	1.88×10^{-5}	4.85×10^{-16}
NMC-1	25.72	419.19	1.67×10^{-5}	8.00×10^{-15}
NMC-3	16.31	285.97	2.45×10^{-5}	7.38×10^{-15}
NMC-5	13.88	506.97	1.38×10^{-5}	2.09×10^{-14}
NMC/C	4.97	48.02	1.46×10^{-4}	4.16×10^{-13}
NMC-Sn/C	3.49	40.37	1.73×10^{-4}	2.49×10^{-13}

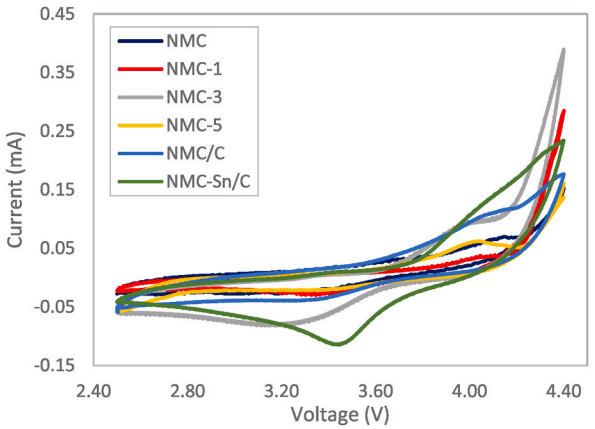

Fig. 9. Cyclic voltammograms of active materials.

Table 6
Potential difference between the anodic and cathodic peaks of active materials.

Sample	Reduction peak (V)	Oxidation peak (V)	ΔE (mV)
NMC	3.18	4.13	950
NMC-1	3.33	4.08	750
NMC-3	3.25	3.97	720
NMC-5	3.32	4.06	740
NMC/C	3.3	4.06	760
NMC-Sn/C	3.45	4.09	640

NMC-Sn/C sample was cycled 50 times at 1C, and the result is shown in Fig. 10. The initial capacity of NMC-Sn/C is 84.5956 mAh/g. After 50 times, NMC/Sn-C maintained capacity of 63.90 mAh/g, showing 75% capacity retention. This shows that Sn doping into NMC provide longer cycle life. This is in agreement with other works, where modification of NMC with 2–3% Sn provided the best electrical performance [18,19,22]. In the current work, 3% Sn doping provided the best electrical performance. Substitution of Co with Sn stabilizes the NMC structure, where Sn stabilizes the octahedral site [16], since Sn has higher bond dissociation energy with oxygen (548 kJ/mol) than that of Co-O (368 kJ/mol) [19]. However, excess amount of Sn can lead to poor electrical performance [19] because Sn is electrochemically inactive and heavier compared to Co. Addition of rice husk derived activated carbon to NMC increasing conductivity and Li^+ diffusion, which is in agreement with the other works [24,25]. However, further study is needed to determine the optimum activated carbon amount, that is above 5 wt%, since it is known that excess carbon coating on NMC can hinder the Li^+ transport, resulting in reduced capacity, but lower amount can result in insufficient coverage [24]. Dual modification with Sn and rice husk activated carbon coating in this work shows better electrochemical properties than single modification. This result is similar to another work [22], where NMC dual modified with Sn doping and Ag coating provided better electrochemical performance than the one with single modification or without modification.

4. Conclusion

Rice husk has been successfully utilized as a cheap activated carbon source. Characterization results showed the activated carbon has semi crystalline structure with surface area of 469.4 m^2/g. Modification of NMC 811 with Sn and rice husk derived activated carbon showed different morphologies but with the same hexagonal crystal system. The varied amount of Sn doping on NMC 811 increased the conductivity, with the optimum shown by 3% Sn (NMC-3, 2.45×10^{-5} S/cm). Modification with rice husk activated carbon coating also showed an increased conductivity (NMC/C, 1.46×10^{-4} S/cm). Dual modification with Sn-doping and rice husk activated carbon coating (NMC-Sn/C) provided the best capacity and conductivity of 84.60 mAh/g and 1.7546×10^{-4} S/cm, respectively. The present results are promising in enhancing the electrochemical performance of nickel rich NMC, especially to reduce the toxic element (Co) and to utilize rice husk waste as a cheap and renewable source for activated carbon. It would be a challenge to work on this future improvement of this material.

Data availability

Data will be made available on request.

CRediT authorship contribution statement

Fiona Angellinnov: Writing - original draft, Investigation, Data curation, Conceptualization. **Achmad Subhan:** Investigation,

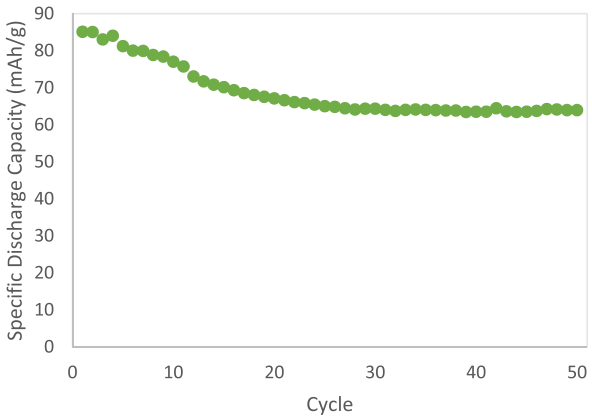

Fig. 10. Cycle performance of NMC-Sn/C.

Data curation. **Alan J. Drew:** Writing - review & editing. **Anne Z. Syahrial:** Writing - review & editing, Supervision, Resources, Project administration, Funding acquisition, Conceptualization.

Declaration of competing interest

The authors declare that they have no known competing financial interests or personal relationships that could have appeared to influence the work reported in this paper.

Acknowledgements

Authors would like to thank Directorate of Research and Community Engagement for financial support under International Publication Index Grants (PUTI Q1) for fiscal 2022–2023 with contract number: NKB-496/UN2.RST/HKP.05.00/2022.

Nomenclature

A	electrode active area
BET	Brunauer Emmett Teller
C	concentration of lithium-ion
EDS	energy dispersive X-ray spectroscopy
F	Faraday constant
FESEM	field emission scanning electron microscope
FTIR	Fourier transform infrared spectroscopy
l	thickness of the electrode sample
LIB	Lithium-Ion Batteries
NMC/C	activated carbon coated NMC
NMC	nickel manganese cobalt
NMC-1	% Sn-doped NMC
NMC-3	3% Sn-doped NMC
NMC-5	5% Sn-doped NMC
NMC-Sn/C	3% Sn-doped activated carbon-coated NMC
PSA	particle size analyzer
R	gas constant
R_{ct}	charge transfer resistance
R_s	solution resistance
T	absolute temperature
TEM	transmission electron microscope
XRD	X-ray diffraction
Z’	real impedance
Z’’	imaginary impedance
σ	conductivity
σ_w	Warburg constant
ω	frequency

Appendix A. Supplementary data

Supplementary data to this article can be found online at https://doi.org/10.1016/j.heliyon.2023.e23199.

References

[1] C. Franco, G. Melica, A. Treville, M.G. Baldi, E. Pisoni, P. Bertoldi, C. Thiel, Prediction of greenhouse gas emissions for cities and local municipalities monitoring their advances to mitigate and adapt to climate change, Sustain. Cities Soc. 86 (2022), 104114, https://doi.org/10.1016/j.scs.2022.104114.
[2] A.G. Mohammed, K.E. Elfeky, Q. Wang, Recent advancement and enhanced battery performance using phase change materials based hybrid battery thermal management for electric vehicles, Renew. Sustain. Energy Rev. 154 (2022), 111759, https://doi.org/10.1016/j.rser.2021.111759.
[3] M.K. Shobana, Metal oxide coated cathode materials for Li ion batteries – a review, J. Alloys Compd. 802 (2019) 477–487, https://doi.org/10.1016/j.jallcom.2019.06.194.
[4] M. Kotal, S. Jakhar, S. Roy, H.K. Sharma, Cathode materials for rechargeable lithium batteries: recent progress and future prospects, J. Energy Storage 47 (2022), 103534, https://doi.org/10.1016/j.est.2021.103534.
[5] L. Lu, X. Han, J. Li, J. Hua, M. Ouyang, A review on the key issues for lithium-ion battery management in electric vehicles, J. Power Sources 226 (2013) 272–288, https://doi.org/10.1016/j.jpowsour.2012.10.060.
[6] A. Hebert, E. McCalla, The role of metal substitutions in the development of Li batteries, part I: cathodes, Mater. Adv. 2 (2021) 3474, https://doi.org/10.1039/d1ma00081k.

[7] S. Chen, X. Zhang, M. Xia, K. Wei, L. Zhang, X. Zhang, Y. Cui, J. Shu, Issues and challenges of layered lithium nickel cobalt manganese oxides for lithium-ion batteries, J. Electroanal. Chem. 895 (2021), 115412, https://doi.org/10.1016/j.jelechem.2021.115412.

[8] M. Malik, K.H. Chan, G. Azimi, Review on the synthesis of LiNixMnyCo1-x-yO2 (NMC) cathodes for lithium-ion batteries, Mater. Today Energy 28 (2022), 101066, https://doi.org/10.1016/j.mtener.2022.101066.

[9] L.J. Li, X.H. Li, Z.X. Wang, H.J. Guo, P. Yue, W. Chen, L. Wu, A simple and effective method to synthesize layered LiNi0.8Co0.1Mn0.1O2 cathode materials for lithium ion battery, Powder Technol. 206 (2011) 353–357, https://doi.org/10.1016/j.powtec.2010.09.010.

[10] H. Sun, Y. Zhang, W. Li, D. Zhang, Q. Wang, B. Wang, Effects of Ag coating on the structural and electrochemical properties of LiNi0.8Co0.1Mn0.1O2 as cathode material for lithium ion batteries, Electrochim. Acta 327 (2019), 135054, https://doi.org/10.1016/j.electacta.2019.135054.

[11] S. Mallick, A. Patel, X.G. Sun, M.P. Paranthaman, M. Mou, J.H. Mugumya, M. Jiang, M.L. Rasche, H. Lopez, R.B. Gupta, Low-cobalt active cathode materials for high-performance lithium-ion batteries: synthesis and performance enhancement methods, J. Mater. Chem. A 11 (2023) 3789, https://doi.org/10.1039/d2ta08251a.

[12] Y. Zhai, W. Yang, D. Ning, J. Yang, L. Sun, G. Schuck, G. Schumacher, X. Liu, Improving the cycling and air-storage stability of LiNi0.8Co0.1Mn0.1O2 through integrated surface/interface/doping engineering, J. Mater. Chem. A 8 (2020) 5234, https://doi.org/10.1039/c9ta13014d.

[13] X. Tan, M. Zhang, J. Li, D. Zhang, Y. Yan, Z. Li, Recent progress in coatings and methods of Ni-rich LiNi0.8Co0.1Mn0.1O2 cathode materials: a short review, Ceram. Int. 46 (2020) 21888–21901, https://doi.org/10.1016/j.ceramint.2020.06.091.

[14] H. Zhang, H. Zhao, M.A. Khan, W. Zou, J. Xu, L. Zhang, J. Zhang, Recent progress in advanced electrode materials, separators and electrolytes for lithium batteries, J. Mater. Chem. A 6 (2018), 20564, https://doi.org/10.1039/c8ta05336g.

[15] G. Shang, Y. Tang, Y. Lai, J. Wu, X. Yang, H. Li, C. Peng, J. Zheng, Z. Zhang, Enhancing structural stability unto 4.5 V of Ni-rich cathodes by tungsten-doping for lithium storage, J. Power Sources 423 (2019) 246–254, https://doi.org/10.1016/j.jpowsour.2019.03.072.

[16] M. Eilers-Rethwisch, M. Winter, F.M. Schappacher, Synthesis, electrochemical investigation and structural analysis of doped Li[Ni0.6Mn0.2Co0.2-xMx]O2 (x = 0, 0.05; M = Al, Fe, Sn) cathode materials, J. Power Sources 387 (2018) 101–107, https://doi.org/10.1016/j.jpowsour.2018.02.080.

[17] M. Jeong, H. Kim, W. Lee, S.J. Ahn, E. Lee, W.S. Yoon, Stabilizing effects of Al-doping on Ni-rich LiNi0.80Co0.15Mn0.05O2 cathode for Li rechargeable batteries, J. Power Sources 474 (2020), 228592, https://doi.org/10.1016/j.jpowsour.2020.228592.

[18] Z. Li, X. Yu, Y. Lv, L. Qi, Y. Ma, H. Zhang, D. Song, X. Shi, L. Zhang, Investigation on the structure and electrochemical performance of LiNi 0.8 Co 0.1 Mn 0.1 O 2 modified with Sn, Electrochim. Acta 400 (2021), 139468, https://doi.org/10.1016/j.electacta.2021.139468.

[19] M. Eilers-Rethwisch, S. Hildebrand, M. Evertz, L. Ibing, T. Dagger, M. Winter, F.M. Schappacher, Comparative study of Sn-doped Li[Ni0.6Mn0.2Co0.2-xSnx]O2 cathode active materials (x = 0-0.5) for lithium ion batteries regarding electrochemical performance and structural stability, J. Power Sources 397 (2018) 68–78, https://doi.org/10.1016/j.jpowsour.2018.06.072.

[20] A. Yalçın, M. Demir, M.O. Güler, M. Gönen, M. Akgün, Synthesis of Sn-doped Li-rich NMC as a cathode material for Li-ion batteries, Electrochim. Acta 440 (2023), 141743, https://doi.org/10.1016/j.electacta.2022.141743.

[21] T.T. Nguyen, U.H. Kim, C.S. Yoon, Y.K. Sun, Enhanced cycling stability of Sn-doped Li[Ni0.90Co0.05Mn0.05]O2 via optimization of particle shape and orientation, Chem. Eng. J. 405 (2021), 126887, https://doi.org/10.1016/j.cej.2020.126887.

[22] H. Sun, J. Wang, Q. Liu, Y. Zhang, D. Zhang, Q. Wang, Z. Li, W. Li, B. Wang, Ag-Sn dual-modified LiNi0.8Co0.1Mn0.1O2 as cathode for lithium storage, J. Alloys Compd. 850 (2021), 156763, https://doi.org/10.1016/j.jallcom.2020.156763.

[23] M. Chaudhary, S. Tyagi, R.K. Gupta, B.P. Singh, R. Singhal, Surface modification of cathode materials for energy storage devices: a review, Surf. Coating. Technol. 412 (2021), 127009, https://doi.org/10.1016/j.surfcoat.2021.127009.

[24] S.J. Sim, S.H. Lee, B.S. Jin, H.S. Kim, Use of carbon coating on LiNi0.8Co0.1Mn0.1O2 cathode material for enhanced performances of lithium-ion batteries, Sci. Rep. 10 (2020), 11114, https://doi.org/10.1038/s41598-020-67818-5.

[25] M. Nanthagopal, P. Santhoshkumar, N. Shaji, S. Praveen, H.S. Kang, C. Senthil, C.W. Lee, Nitrogen-doped carbon-coated Li[Ni0.8Co0.1Mn0.1]O2 cathode material for enhanced lithium-ion storage, Appl. Surf. Sci. 492 (2019) 871–878, https://doi.org/10.1016/j.apsusc.2019.06.242.

[26] G. Chen, B. Peng, R. Han, N. Chen, Z. Wang, Q. Wang, A robust carbon coating strategy toward Ni-rich lithium cathodes, Ceram. Int. 46 (2020) 20985–20992, https://doi.org/10.1016/j.ceramint.2020.05.160.

[27] X. Li, Z. Hua, Z. Li, M. Shao, F. Lü, P.J. He, Preparation and application of hierarchical porous carbon materials from waste and biomass : a review, Waste Biomass Valoriz. 12 (2021) 1699–1724, https://doi.org/10.1007/s12649-020-01109-y.

[28] R. Pode, Potential applications of rice husk ash waste from rice husk biomass power plant, Renew. Sustain. Energy Rev. 53 (2016) 1468–1485, https://doi.org/10.1016/j.rser.2015.09.051.

[29] S.S. Shukla, R. Chava, S. Appari, A. B, B.V.R. Kuncharam, Sustainable use of rice husk for the cleaner production of value-added products, J. Environ. Chem. Eng. 10 (2022), 106899, https://doi.org/10.1016/j.jece.2021.106899.

[30] M.J. Saad, C.C. Hua, S. Misran, S. Zakaria, M.S. Sajab, M.H. Abdul Rahman, Rice husk activated carbon with NaOH activation: physical and chemical properties, Sains Malays. 49 (2020) 2261–2267, https://doi.org/10.17576/jsm-2020-4909-23.

[31] K.C. Kam, A. Mehta, J.T. Heron, M.M. Doeff, Electrochemical and physical properties of Ti-substituted layered nickel manganese cobalt oxide (NMC) cathode materials, J. Electrochem. Soc. 159 (2012) A1383–A1392, https://doi.org/10.1149/2.060208jes.

[32] L. Shrestha, M. Thapa, R. Shrestha, S. Maji, R. Pradhananga, K. Ariga, Rice husk-derived high surface area nanoporous carbon materials with excellent iodine and methylene blue adsorption properties, C 5 (2019) 10, https://doi.org/10.3390/c5010010.

[33] Y. Guo, D.A. Rockstraw, Activated carbons prepared from rice hull by one-step phosphoric acid activation, Microporous Mesoporous Mater. 100 (2007) 12–19, https://doi.org/10.1016/j.micromeso.2006.10.006.

[34] Y. Chen, Y. Zhu, Z. Wang, Y. Li, L. Wang, L. Ding, X. Gao, Y. Ma, Y. Guo, Application studies of activated carbon derived from rice husks produced by chemical-thermal process - a review, Adv. Colloid Interface Sci. 163 (2011) 39–52, https://doi.org/10.1016/j.cis.2011.01.006.

[35] K. Le Van, T.T.L. Thi, Activated carbon derived from rice husk by NaOH activation and its application in supercapacitor, Prog. Nat. Sci.: Mater. Int. 24 (2014) 191–198, https://doi.org/10.1016/j.pnsc.2014.05.012.

[36] L.J. Kennedy, J.J. Vijaya, G. Sekaran, Effect of two-stage process on the preparation and characterization of porous carbon composite from rice husk by phosphoric acid activation, Ind. Eng. Chem. Res. 43 (2004) 1832–1838, https://doi.org/10.1021/ie034093f.

[37] F.T. Li, J. Ran, M. Jaroniec, S.Z. Qiao, Solution combustion synthesis of metal oxide nanomaterials for energy storage and conversion, Nanoscale 7 (2015), 17590, https://doi.org/10.1039/c5nr05299h.

[38] F. Deganello, A.K. Tyagi, Solution combustion synthesis, energy and environment: best parameters for better materials, Prog. Cryst. Growth Char. Mater. 64 (2018) 23–61, https://doi.org/10.1016/j.pcrysgrow.2018.03.001.

[39] K.R. Prakasha, A.S. Prakash, A time and energy conserving solution combustion synthesis of nano Li1.2Ni0.13Mn0.54Co0.13O2 cathode material and its performance in Li-ion batteries, RSC Adv. 5 (2015), 94411, https://doi.org/10.1039/c5ra19096g.

[40] T. Ohzuku, A. Ueda, M. Nagayama, Electrochemistry and structural chemistry of LiNiO2 (R3m) for 4 volt secondary lithium cells, J. Electrochem. Soc. 140 (1993) 1862–1870, https://doi.org/10.1149/1.2220730.

[41] G.X. Wang, S. Zhong, D.H. Bradhurst, S.X. Dou, H.K. Liu, Synthesis and characterization of LiNiO2 compounds as cathodes for rechargeable lithium batteries, J. Power Sources 76 (1998) 141–146, https://doi.org/10.1016/S0378-7753(98)00153-0.

[42] J. Wilcox, S. Patoux, M. Doeff, Structure and electrochemistry of LiNi1/3Co1/3−yMyMn1/3O2 (M=Ti, Al, Fe) positive electrode materials, J. Electrochem. Soc. 156 (2009) A192–A198, https://doi.org/10.1149/1.3056109.

[43] K. Yu, J. Li, H. Qi, C. Liang, High-capacity activated carbon anode material for lithium-ion batteries prepared from rice husk by a facile method, Diam. Relat. Mater. 86 (2018) 139–145, https://doi.org/10.1016/j.diamond.2018.04.019.

[44] L. Wang, J. Liang, X. Zhang, S. Li, T. Wang, F. Ma, J. Han, Y. Huang, Q. Li, An effective dual-modification strategy to enhance the performance of LiNi0.6Co0.2Mn0.2O2cathode for Li-ion batteries, Nanoscale 13 (2021) 4670, https://doi.org/10.1039/d0nr09010g.